Journal of Materials Chemistry C

ROYAL SOCIETY OF CHEMISTRY

PAPER

View Article Online
View Journal

Cite this: DOI: 10.1039/d5tc04053a

Near-infrared fluorescent Ag_2S quantum dots stabilized by penicillamine enantiomers: influence of ligand chirality on linear and nonlinear optical properties and toxicity

Jakub Tracz, [a] Agnieszka Siomra, [b] Zuzanna Kaźmierczak, [cde] Kostiantyn Rokush, [c] Robert Tomala, [f] Marek Samoć, [b] Jiří Pfleger, [g] Marcin Nyk [b] and Marta Gordel-Wójcik *[ag]

We present hydrothermal synthesis and comprehensive physicochemical characterization of water-soluble Ag_2S quantum dots (QDs) emitting in the second near-infrared biological window (NIR-II), stabilized by chiral ligands: L- and D-penicillamine (Pen). By systematically optimizing reaction temperature, time, and the Ag : S ratio, we significantly improved the photophysical properties of the QDs. The obtained Ag_2S/Pen QDs exhibited NIR-II emission ($\lambda_{EM.} \sim 1040$ nm) with a fair quantum yield (QY = 1.1%), high colloidal stability, low cytotoxicity, and fluorescence lifetime reaching 84 ns in aqueous media. The use of enantiomerically pure and racemic variants of Pen allowed us to investigate the influence of stereoisomer configuration on morphology and consequently, linear and nonlinear optical (NLO) properties of the QDs. Spectrally-resolved NLO study using a femtosecond laser Z-scan technique showed the presence of two-photon absorption (2PA) with a peak cross section reaching $\sigma_2 \sim 511$ GM (Goeppert–Mayer units) for Ag_2S/D-Pen excited at $\lambda_{EXC.} = 824$ nm and 260 GM ($\lambda_{EXC.} = 950$ nm) for Ag_2S/L-Pen, respectively. Biocompatibility studies in THP-1 macrophages and HLMEC endothelial cells revealed favorable tolerance profiles for Ag_2S/Pen QDs, particularly in immune cells. Notably, macrophages maintained high viability and even showed enhanced metabolic activity, while endothelial cells exhibited good tolerance at lower concentrations, supporting the potential of these QDs for biomedical applications involving immune and vascular systems. These findings demonstrate that the structure of surface ligands plays a key role in controlling the structural and optical properties of Ag_2S QDs, providing insights for the design of NIR fluorescent nanomaterials for biomedical and photonic applications.

Received 14th November 2025,
Accepted 3rd March 2026

DOI: 10.1039/d5tc04053a

rsc.li/materials-c

Introduction

Quantum dots (QDs) are a class of semiconductor nanomaterials characterized by the quantum confinement effect arising from their zero-dimensional structure. This confinement leads to discrete energy levels and size-dependent optical and electrical properties, making QDs highly versatile for applications across diverse disciplines.[1–5] Their application in theranostics, particularly in fluorescence imaging, necessitates specific characteristics such as near-infrared (NIR) emission for deep-tissue imaging, long fluorescence lifetimes, high quantum yield (QY), resistance to photobleaching, and low toxicity.[6] While numerous studies highlighted the exceptional optical properties of QDs, the issue of toxicity, critical for their particle implementation in biological imaging, is often overlooked. For instance, heavy metal-based QDs, such as PbS, demonstrate high QY values exceeding 40% in the NIR-II spectral range (1000–1700 nm).[7,8]

[a] Faculty of Chemistry, University of Wrocław, 14.p F. Joliot-Curie Street, 50-383, Wrocław, Poland. E-mail: marta.gordel-wojcik@uwr.edu.pl
[b] Institute of Advanced Materials, Faculty of Chemistry, Wrocław University of Science and Technology, Wyb. Wyspiańskiego 27, 50-370, Wrocław, Poland
[c] Laboratory of Phage Molecular Biology, Hirszfeld Institute of Immunology and Experimental Therapy, Polish Academy of Sciences, Weigla 12, 53-114 Wrocław, Poland
[d] Research and Development Center, Regional Specialist Hospital in Wrocław, Kamieńskiego 73A, 51-124 Wrocław, Poland
[e] Faculty of Medicine, Department of Preclinical Sciences, Pharmacology and Medical Diagnostics, Wrocław University of Science and Technology, Hoene-Wrońskiego 13 c, 58-376 Wrocław, Poland
[f] Institute of Low Temperature and Structure Research, Polish Academy of Sciences, Okólna 2, Wrocław 50-422, Poland
[g] Department of Polymers for Electronics and Photonics, Institute of Macromolecular Chemistry Czech Academy of Sciences, Heyrovského nám. 2, 16206 Prague 6, Czech Republic

However, their intrinsic toxicity significantly restricts biomedical applications. Consequently, the development of alternative QDs, such as Ag_2S QDs with both low toxicity and NIR-II emission, is of paramount importance for *in vivo* imaging. The emission properties of such QDs can be precisely tailored through the selection of stabilizing ligands and optimized synthesis conditions. Despite their relatively high biocompatibility and low toxicity, attributable to the extremely low solubility of Ag_2S in aqueous environments, which limits Ag^+ ion release and mitigates cytotoxic effects,[9] a major challenge persists in the inherently low QY of most fluorescent probes operating in the NIR range. Low QY values are typically associated with short fluorescence lifetimes in the water phase (10–55 ns[10,11]). In the case of the organic phase, rather longer lifetimes in the range of 50–180 ns were reported.[12–17] Prolonged fluorescence lifetimes of QDs offer several benefits, including reduced cellular exposure to the intense excitation light typically required for conventional fluorophores. This enables observation of living systems over extended periods without causing cellular damage. Moreover, since natural cellular autofluorescence decays rapidly, the prolonged fluorescence signal enhances contrast, making it easier to distinguish true signals from background noise and significantly improving detection accuracy. Conventional organic fluorophores exhibit rapid fluorescence decay with lifetimes below 20 ns, whereas QDs possess sufficiently prolonged emission characteristics from nanoseconds to microseconds, ensuring that by the time autofluorescence signals of biological species have dissipated, QDs continue to emit photons. This property facilitates the acquisition of clear and stable optical signals, making QDs particularly suitable for high-contrast and long-duration bioimaging applications.[18,19] QDs luminescence lifetime can be further modulated by improving crystal quality, the nature of surface traps, ligand shell composition, and the introduction of dopants or core–shell structures that separate excitons.[20,21] Surface trap states can have a dual effect on emission dynamics: shallow traps may act as intermediate states that prolong fluorescence lifetime, while deep traps often serve as non-radiative recombination centers that quench emission. Proper surface passivation through optimized ligand coverage helps minimize deep traps and stabilize radiative pathways, enhancing both lifetime and QY. This phenomenon has been applied in time-gated imaging, where the unique features of QDs lead to a significant enhancement in cellular imaging.[22] The long fluorescence lifetime QDs can be successfully employed as nanoprobes in time-resolved fluorescence (TRF) based nanosensors, with potential applications in biological measurements. QDs demonstrate significant potential for cell detection with improved selectivity and sensitivity, and these applications can be extended to *in vivo* cell imaging, particularly by utilizing fluorescence lifetime imaging microscopy (FLIM) techniques. Recent studies have demonstrated that TRF spectroscopy is a sensitive tool for detecting and quantifying multiple interactions between QDs and other molecules.[23,24]

Among the advantages of QDs is the possibility of their application in two-photon fluorescence microscopy (TPFM), which offers several advantages over conventional one-photon excited emission, such as improved resolution, deeper tissue imaging, and reduced phototoxicity and photobleaching.[25,26] Especially useful in this context are materials capable of both excitation and emission in the NIR range, such as Ag_2S QDs, which can serve as excellent fluorescent markers.[27] It should be mentioned that, apart from two-photon excited fluorescence, the 2PA nanomaterials often exhibit other NLO properties, such as one-photon absorption saturation (1PA SAT) and reverse saturable absorption (RSA), making them attractive for a wide range of applications in NLO devices.[28–32] Precise characterization of the NLO parameters (*e.g.*, using the femtosecond laser Z-scan technique) enables tailoring of materials for specific applications.

The low QY and short lifetimes of Ag_2S QDs are consistent with the presence of surface-related trap states discussed above, which facilitate non-radiative relaxation channels. Consequently, various strategies have been explored to enhance these parameters, including different QDs synthesis methods,[4] surface passivation with wide-band-gap-materials,[15] cation doping,[33] or chemical etching.[34] Notably, high QY and prolonged fluorescence lifetimes of Ag_2S QDs have been achieved in several studies, with one of the reports demonstrating a QY of 2.3% and lifetimes up to 1200 ns using an organic-phase synthesis method.[16] In another study,[34] the lifetime of Ag_2S QDs reached nearly 1700 ns through a sonochemical etching process. An interesting methodology was proposed by Santos *et al.*,[15] who created so-called "*superdots*" based on Ag_2S by irradiating chloroform-dispersed Ag_2S dots with 50 fs laser pulses. This led to the formation of a protective AgCl shell, which increased the QY from 0.13% to 10.70% and extended the fluorescence lifetime from 200 ns to 2100 ns. Additionally, with specific coatings of Ag_2S QDs, the following lifetimes were obtained: 32.8 ns for TGA-coated QDs (emission λ = 1000 nm),[35] 33.4 ns and 19.7 ns for *N*-isobutyryl-L-/D-cysteine coatings, respectively (emission λ = 1060 nm),[36] and for diethyldithiocarbamate (DDTC) (1-dodecanethiol as coating) by thermal decomposition 58 ns and more for higher temperatures (emission λ = 1052 nm).[14]

Although substantial progress has been made in the development of NIR-II-emitting Ag_2S QDs, their hydrophobic surface, resulting from organic-phase synthesis, remains an obstacle to their direct use in biological environments.[37] To address this challenge, a promising alternative is the direct synthesis of hydrophilic Ag_2S QDs in an aqueous phase. This approach, coupled with the use of suitable coatings and optimized synthesis conditions, enables effective encapsulation of the Ag_2S QD core while maintaining desirable optimal emission properties in the NIR-II range.[4] However, it is important to avoid emissions at around 1200 nm and above 1400 nm within the NIR-II region, as water molecules exhibit strong absorption of light resulting from bending and stretching vibrations of the hydroxyl group.[38–40] This absorption attenuates the photoluminescence of QDs and can significantly interfere with the imaging application.

Chirality is a fundamental characteristic of many biological systems and plays a crucial role in regulating essential

physiological functions. The introduction of chirality into nanoscale systems has attracted growing scientific interest, and various types of chiral nanomaterials have been reported, including gold nanorods,[41] silver nanoparticles,[42] carbon nanoparticles,[43] and ZnO layers.[44] Among them, chiral QDs stand out as promising candidates for applications in biological sensing,[45] chiral catalysis, quantum optics, and medicine due to their ease of manipulation, tunable optical properties, and strong circular dichroism (CD) signals in the UV range.[46–49] Although most QDs are not chiral, chirality in these materials can be efficiently induced by chiral ligands that passivate their surface.[48–50] One of the first demonstrations of chiroptical activity induction in QDs was reported by the group of Moloney.[51] They obtained chiral CdS QDs by microwave heating, using racemic and enantiomeric forms of D- and L-penicillamine (D-Pen and L-Pen, respectively) as stabilizers. This work initiated the development of various methods for synthesizing QDs using different chiral molecules. The use of amino acids (*e.g.*, cysteine (Cys) and penicillamine (Pen)) and peptides as chiral ligands for QD synthesis has become particularly widespread.[52] Despite the time that has passed since Moloney's studies, to our knowledge, only one publication has focused on QDs with an Ag_2S core stabilized with D-Pen.[53] However, that work did not address the chiral characteristics of the studied nanoparticles.

The introduction of chirality into QDs opens new perspectives in developing advanced optical nanosensors, while simultaneously raising questions about the impact of chiral QD configurations on their properties. Similar to proteins or certain drugs, chiral nanostructures may exhibit varying biological activities depending on their conformation. For example, the transactivator protein of the human immunodeficiency virus type 1 (HIV-1) shows a clear preference for D-Pen over L-Pen.[54] Investigations on graphene quantum dots (GQDs) have shown that L-GQDs exhibit better biocompatibility than D-GQDs, which reflects a similar trend observed for L- and D-enantiomers of free Cys.[55] In turn, investigations on NIBC-capped D-/L-Ag_2S QDs[36] revealed significant differences in their interactions with serum proteins, which additionally affect cellular uptake. It was found that D-Ag_2S QDs adsorbed significantly more proteins than L-Ag_2S QDs, exhibited more efficient renal elimination and promoted accumulation in tumor tissues, while L-Ag_2S QDs were retained longer in the blood. Surface chirality also affects cytotoxicity, as demonstrated in the work of Li *et al.*,[56] where CdTe/L-GSH QDs were more cytotoxic than CdTe/D-GSH QDs.

In this study, we present a new approach for synthesizing colloidal Ag_2S QDs coated with Pen, using a simple one-pot hydrothermal method. Inspired by the dynamic development of chiral QDs research, we analyzed the effects of various synthesis conditions on the optical properties of QDs with coatings based on the D-/L-, and racemic (*Rac*-) variants of Pen. The results enabled the synthesis of Ag_2S QDs emitting in the NIR-II range, characterized by surprisingly long fluorescence lifetimes, a critical parameter for applications in fluorescence imaging. Besides, the QDs synthesized in this study exhibit 2PA properties across a broad spectral range (approximately 800–1400 nm), which is significantly wider than that observed for Ag_2S QDs stabilized with mercaptopropionic acid in our earlier work.[57] To further evaluate their potential application, cytotoxicity assays were conducted, confirming low toxicity and indicating high suitability for biological and biomedical applications.

Materials and methods

Synthesis

For the Ag_2S/Pen QDs synthesis, all chemicals were procured from Merck. During the synthesis, the pH was monitored with METTLER TOLEDO series FiveGO F2 pH-meter with LE438 IP67 electrode. Ag_2S QDs were synthesized according to previous protocol with some modifications.[58]

The reactions were carried out under a nitrogen atmosphere. In a Schlenk flask, 75 mL and 25 mL of water, along with aqueous solutions of NaOH and CH_3COOH (each at a concentration of 1 M), were degassed by applying vacuum for 20 min. Subsequently, the solutions were subjected to nitrogen purging for 10 min under a nitrogen-saturated atmosphere. Further synthesis steps were carried out in a three-necked flask equipped with a magnetic stir bar, under a protective plastic dome.

Herein, 74.6 mg Pen (0.500 mmol) was dissolved in 75 mL of deoxygenated water. The pH of the solution was adjusted to 12 by the addition of NaOH and CH_3COOH solutions. Subsequently, 42.5 mg of $AgNO_3$ (0.250 mmol) was added, which resulted in the formation of a yellow coloration that disappeared immediately upon stirring. The pH was readjusted to 12. Next, the flask, fitted with a reflux condenser, was immersed in an oil bath and heated to the desired temperature while maintaining a continuous flow of nitrogen gas. A solution of Na_2S (0.062 mmol, 15 mg) in 25 mL of water was added dropwise to the reaction mixture *via* syringe. This addition caused a color change to light yellow or orange. As the reaction proceeded, the solution progressively darkened. Upon completion of the reaction, the reaction flask was allowed to cool to ambient temperature and the contents were transferred to a separate vessel for further cooling. The resulting solution exhibited a brown or orange hue. The reaction mixture was filtered through a 0.22 μm syringe filter into a receptacle crafted from darkened glass, yielding a visually clear, light-brown filtrate.

The final purification step involved centrifugation by ethanol precipitation. For this purpose, the colloidal QDs solution was mixed with fresh ethanol in a 1 : 1 (v/v) ratio in a centrifuge tube and centrifuged for 5 min at 14 000 rpm (23 666 rcf.). The precipitate collected on the tube walls was dispersed in 10 mL of water, resulting in approximately twice the concentration of the QD solution.

Chiral Ag_2S QDs coated with Pen enantiomers were synthesized in water using the hydrothermal method, with the slow addition of Na_2S as the sulfur source. The choice of Na_2S is because Pen is a stable amino acid at the investigated temperatures and cannot supply S^{2-} ions during the formation of the QD core. Therefore, Na_2S was used as the sulfur source in this

Table 1 Synthesis conditions of Ag_2S QDs along with their measured properties and parameters. Samples marked with an asterisk (*) were not purified by centrifugation in an ethanol:water solution

Coating/sample number	Ag : S	T [°C]	$pH_{(after)}$	Zeta pot. (mV)	Size (nm)	$\tau_{average}$ 3-exponential decay [ns]	Correlation coefficient $\chi^2_{3\text{-exponential decay}}$	λ_{cutoff} [nm]	$\lambda_{em,\ max}$ [nm]
D-Pen									
D-2a	2	50	11.7	−26.30	4.3 ± 0.7	30.9	1.0990	970	1030
D-2b	2	90	11.6	−11.78	4.6 ± 1.1	55.9	1.0670	962	1041
D-4a*	4	50	11.6	−26.63	4.3 ± 0.8	11.3	1.1050	786	1009
D-4b	4	90	11.6	−36.16	3.6 ± 0.7	71.1	1.0450	844	1037
Rac-Pen									
R-2a*	2	50	11.7	−29.95	5.8 ± 1.2	14.1	1.0700	954	1013
R-2b	2	90	11.6	−14.76	3.9 ± 0.9	13.6	1.1540	956	1053
R-4a*	4	50	11.6	−34.99	3.7 ± 0.6	8.9	1.1800	944	1012
R-4b	4	90	11.4	−34.33	3.6 ± 0.7	65.5	1.0360	>1100	1018
L-Pen									
L-2a	2	50	11.7	−41.18	3.6 ± 0.6	48.0	1.0620	950	1029
L-2b	2	90	11.6	−25.28	4.2 ± 0.9	25.6	1.0990	943	1062
L-4a*	4	50	11.6	−42.96	3.7 ± 0.6	11.1	1.2210	757	1005
L-4b	4	90	11.4	−31.92	3.4 ± 0.7	84.3	1.0570	945	1037

study, with a variable Ag : S molar ratio of 2 and 4. Syntheses were carried out under a nitrogen atmosphere, changing the reaction parameters such as temperature (50 or 90 °C), Ag : S ratio, and reaction time to determine the optimal conditions for QDs synthesis (details in Table 1 and Table S1, Section S4 in SI). In each case, the Pen : Ag ratio was constant and equal to 2 : 1.

From here on, individual samples are designated as D-, R- or L-type, where the prefix (D, R, or L) represent the specific configuration of the Pen coating. The first number (2 or 4) indicates the Ag : S precursor ratio, while the letter (a or b) corresponds to the synthesis temperature – 50 °C for "a" and 90 °C for "b". For example, sample D-4a* refers to the sample synthesized using an Ag : S precursor ratio of 1 : 4 at 50 °C. The asterisk "*" indicates that the sample could not be purified by centrifugation in an ethanol:water solution.

All experiments were carried out in an alkaline environment at pH 12.0 before addition of Na_2S. The use of an alkaline environment is due to the fact that the thiol group of Pen is characterized by a pK_a value of ~10.5.[59] In this pH range, both the thiol and carboxyl groups are deprotonated, assuming a negatively charged form, while the amino group remains mostly uncharged. As is well known, silver(I) ions, classified as soft acids, form preferentially strong complexes with sulfur-containing ligands, thus the silver–sulfur bond is not disturbed by the carboxyl group.[58,60,61] This pH value was also indicated by Moloney[62] as necessary for the formation of chiral CdS QDs with Pen.

Methods

Optical characterization

The absorption spectra of the solutions were measured in a 1 cm quartz cuvette using a Shimadzu UV-1900i spectrophotometer.

Fluorescence lifetime and emission spectra of Ag_2S QDs in water were measured using the TCSPC technique with FluoTime 300 (PicoQuant, Germany) connected to a tunable Solea White Supercontinuum laser excitation source set to 500 nm. Full width at half maximum of the instrument response function was ~200 ps. The emission and emission lifetimes were measured using a Hamamatsu thermoelectric cooled NIR-PMT unit H10330C-45 operating in the 950–1400 nm range.

The QY was determined using indocyanine green (ICG) as a reference standard (QY = 10.6% in DMSO). The measurements were performed using an FLS 980 fluorescence spectrometer (Edinburgh Instruments Ltd) with a Czerny–Turner monochromator configuration. A xenon lamp (XE1, 250 nm) served as the excitation source, and emission was detected using a NIR-PMT detector (maximum range: 1200 nm). Measurements were conducted in a 10 mm path length quartz cuvette.

CD spectra were obtained on a JASCO J-1500 spectropolarimeter in a spectral range of 180–400 nm. The measurement step was 1 nm and the scanning speed was 100 nm min^{-1}. Measurements were performed at room temperature and all samples were diluted in water to achieve concentration of approximately 0.5 mmol mL^{-1}.

The NLO properties of the studied Ag_2S QDs were investigated experimentally using the femtosecond laser Z-scan technique. The measurements were performed with a tunable femtosecond laser system, consisting of a Coherent® Astrella ultrafast regenerative amplifier operating as the 800 nm pump, generating ~55 fs laser pulses at a 1 kHz repetition rate, followed by a TOPAS-PRIME optical parametric amplifier providing wavelengths in a broad spectral range from 600 to 1600 nm, as described previously by our group.[63]

Structural characterization

The hydrodynamic size of nanoparticles in colloidal solutions and the zeta potential were measured using the Malvern Zetasizer Ultra Red instrument, employing electrophoretic light scattering methodology based on the Smoluchowski model.

The nanoparticle size characterization was conducted using a FEI Tecnai G2 20 X-TWIN High Resolution Transmission Electron Microscope. Solutions were deposited onto TEM grids, dried, and subsequently imaged.

ATR FT-IR spectra were collected using a Bruker Vertex 70v Fourier transform infrared spectrometer equipped with an air-cooled DTGS detector and a diamond attenuated total reflection infrared cell at 2 cm^{-1} resolution and 64 scans at room temperature. The samples were applied onto the diamond crystal in liquid form and subsequently dried under vacuum prior to measurement.

Powder X-ray diffraction (XRD) patterns were recorded using a PANalytical AERIS diffractometer. The measurement was performed in the 2θ range of 20–70°, using Cu Kα_1 radiation (λ = 1.5406 Å) with the counting time of 300 s and the step of 0.02°. The reference pattern was taken from International Centre for Diffraction Data (ICDD) card no. 14-0072 (Ag_2S).

Cell culture

Tested cell lines, THP-1 obtained from the American Type Culture Collection (ATCC, Rockville, Maryland, USA) and HLMEC (human lung microvascular endothelial cells) established in the laboratory of C. Kieda (Centre National de la Recherche Scientifique, patent 99-16169), were maintained at the Cell Culture Collection of the Hirszfeld Institute of Immunology and Experimental Therapy, Polish Academy of Science (Wrocław, Poland).

Undifferentiated THP-1 cells were cultured in tissue culture flasks and incubated at 37 °C and 5% CO_2 humidified atmosphere in RPMI supplemented with 15% (v/v) FBS and 50 μM β-mercaptoethanol. HLMEC cells were cultured in RPMI medium supplemented with 15% (v/v) FBS. Both cell lines were maintained at a density of 5×10^5 cells per mL, and the media was changed twice per week.

MTT cytotoxicity assay

For cytotoxicity evaluation, two cell models were applied: human acute monocytic leukemia cell line (THP-1) and human lung microvascular endothelial cells (HLMEC). THP-1 cells were seeded in 96-well plates at a density of 5×10^4 cells per well in culture medium and cultured in a humidified atmosphere containing 5% CO_2 at 37 °C. HLMEC cells were seeded at a density of 2.5×10^4 cells per well under identical culture conditions. Prior to QDs exposure, THP-1 cells were differentiated into macrophages by treatment with 50 ng mL^{-1} phorbol-12-myristate-13-acetate (PMA) for 24 hours in RPMI medium.

Following differentiation, both cell types were exposed to various concentrations of Ag_2S QDs stabilized with D-/L-Pen (1, 0.1, 0.01, and 0.001 mg mL^{-1}) for 48 hours. Control cells were treated with the vehicle used for QD dilution (water). Cell morphological changes after exposure to QDs were monitored using inverted light microscopy. Cell viability was quantitatively determined using the MTT [3-(4,5-dimethylthiazol-2-yl)-2,5-diphenyltetrazolium bromide]. After the 48-hour exposure period, 10 μL of MTT solution was added to each well, and plates were incubated at 37 °C under 5% CO_2 for 2 hours. Subsequently, 100 μL of lysis buffer (20% SDS, 50% *N*,*N*-dimethylformamide, pH 4.7) was added to each well to solubilize the formazan crystals, followed by a 2-hour incubation period. Cell viability was assessed by measuring the optical density at 570 nm (OD_{570}) using an automated microplate reader (Synergy HTX multi-mode reader, Agilent Technologies Inc., Santa Clara, CA, USA). Results were expressed as percentage of cell viability after normalizing the data by untreated control cells. Data represent results from three independent experiments.

Statistical analysis

Statistical analysis was performed using GraphPad Prism 10 (GraphPad Software Inc., San Diego, CA, USA), and carried out by two-way ANOVA-Tukey's *post hoc*.

Results and discussion

The crystal structure of dried QDs solutions was analyzed using XRD. Typically, due to the small size of QDs and the presence of surface ligands, the directly obtained XRD patterns were weak and exhibited broad, undistinguishable peaks.[64,65] To improve the clarity of diffraction patterns, the sample was subjected to heat treatment in a nitrogen atmosphere at 180 °C for 1 hour, which led to the decomposition of surface compounds (D-Pen) and removal of organic residues. After this process, the positions and relative intensities of all diffraction peaks closely matched the monoclinic α-Ag_2S structure, in agreement with the reference pattern ICDD No. 14-0072, (marked with red lines in Fig. S1 and Section S1 in SI), suggesting the as-prepared products were indeed Ag_2S nanocrystals.

The ATR FT-IR spectroscopy was used to identify the functional groups present in Ag_2S/L-Pen QDs. Fig. 1(b) shows the representative FT-IR spectrum of Ag_2S/L-Pen QDs along with the spectrum of the zwitterionic form of Pen (Fig. 1(a)). A weak-intensity band at 2512 cm^{-1}, observed in the spectrum of free L-Pen attributed to the ν(S–H) stretching vibrations,[53,66,67] disappears in the spectrum of Ag_2S/L-Pen QDs.

Additionally, the FT-IR spectrum of Ag_2S/L-Pen QDs exhibits characteristic bands at 1631 cm^{-1} and 1382 cm^{-1}, corresponding to the asymmetric and symmetric stretching vibrations of the carboxylate (COO^-) group, respectively. The presence of these bands confirms the ionic form of L-Pen on the Ag_2S surface. Similar to Ag_2S/L-Cys QDs described in our previous study,[58] a shift of the $\nu_{as}(COO^-)$ band to higher frequencies and the $\nu_s(COO^-)$ band to lower frequencies is observed compared to free Pen. Similarly, in the case of copper sulfide QDs, substantial shifts in vibrational modes and peak merging were observed in the FT-IR spectrum compared to that of free L-Pen ligands.[50]

Pen or its structural analog Cys, exhibits a strong affinity for metal surfaces due to the presence of thiol, carboxyl (or carboxylate), and amino (or ammonium) groups, which can interact with the metal surface. Under the reaction conditions (pH = 12), the participation of the COO^- group in coordination

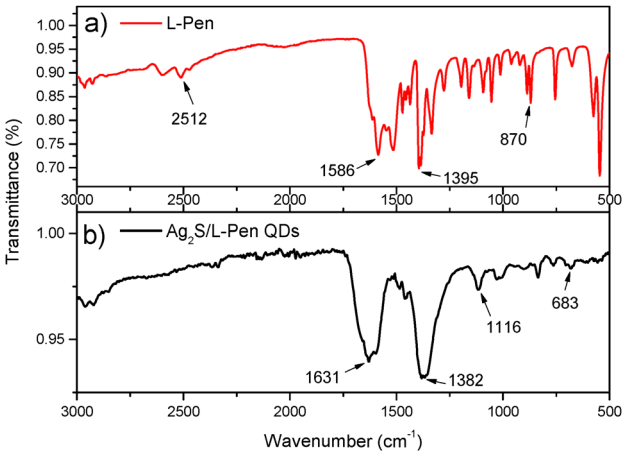

Fig. 1 FT-IR spectra of (a) zwitterionic form of L-Pen and (b) Ag_2S/L-Pen QDs.

is expected; however, in such a case, a shift of $\nu_s(COO^-)$ towards higher energies would be anticipated, as also mentioned in our previous study.[58] Based on an analogy to L-Cys, FT-IR spectra of Ag_2S/Pen QDs indicate that under the adopted reaction conditions, Pen acts as a passivating agent on the surface of Ag_2S QDs.

Fig. 2(a), (b) and (d) presents HR-TEM images of Ag_2S QDs capped with D-Pen, *Rac*-Pen, and L-Pen, respectively, for which the following reaction conditions were used: $T = 90$ °C, Ag : S = 2 and $t = 120$ min (corresponding to samples D-2b, R-2b and L-2b in Table 1). In contrast, Fig. 2(c) shows HR-TEM images of Ag_2S/L-Pen QDs obtained with an increased Ag : S molar ratio of 4 (sample L-4b in Table 1). Most nanoparticles exhibit a narrow size distribution, with diameters ranging from approximately 3.4 to 5.8 nm. The size distribution histograms (shown in the insets of the respective TEM images), calculated by measuring over 200 particles, present the average size and standard deviation of the QDs synthesized under specific conditions (summarized in Table 1). It is noteworthy that increasing the Ag : S molar ratio during reaction from 2 to 4 led to a decrease in the average particle size and resulted in a significantly narrower size distribution 2c)).

A crucial factor influencing the optical properties of the synthesized QDs is their colloidal stability. In the case of Ag_2S QDs stabilized with D-/L-Pen and synthesized under highly alkaline conditions (pH = 12), all carboxyl groups were deprotonated. This process ensured electrostatic repulsion between the nanoparticles, resulting in a negative zeta potential for all QDs (Table 1).

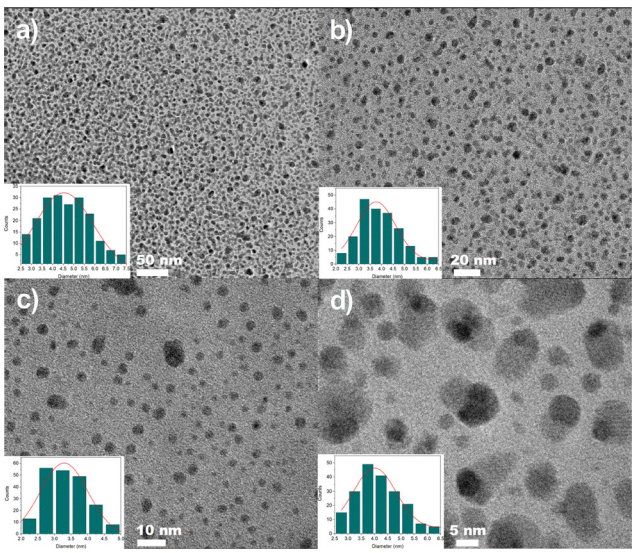

Fig. 2 Representative HR-TEM images and the corresponding size distribution histograms of the colloidal Ag_2S QDs, coated with (a) D-Pen (sample D-2b) (average size 4.6 ± 1.1 nm), (b) *Rac*-Pen (sample R-2b) (average size 3.9 ± 0.9 nm), (c) L-Pen (sample L-4b) (average size 3.4 ± 0.7 nm) and (d) L-Pen (sample L-2b) (average size 4.2 ± 0.9 nm).

Chiroptical properties of Ag_2S/Pen

CD absorption spectroscopy was used to investigate the optical activity of Ag_2S QDs, providing insights into their chiroptical properties (Fig. 3). As predicted, the CD spectra of free D-/L-Pen exhibited mirror images of each other, with distinct maxima/minima at 225, 204 and ~190 nm wavelengths (purple and yellow curve, respectively, in Fig. 3). In contrast, the CD spectra Ag_2S QDs stabilized with D-/L-Pen are significantly more complex compared to the spectral characteristics of the free amino acids (black and blue curve, respectively, in Fig. 3), while the QDs prepared with a *Rac* mixture showed only a weak signal (red curve, Fig. 3). The hypsochromic shift of the CD peak of Pen from 225 nm towards 215 nm upon attachment to QDs suggests strong interactions between the ligand and the QDs surface. Additionally, a slight red-shift of the peaks around ~190 nm in the CD spectra of QDs confirms structural changes resulting from ligand binding. Moreover, there is a new weaker band developed centered at about 245 nm.

To exclude the possibility of intrinsic chirality of the QDs themselves, we investigated Ag_2S QDs coated with another thiol

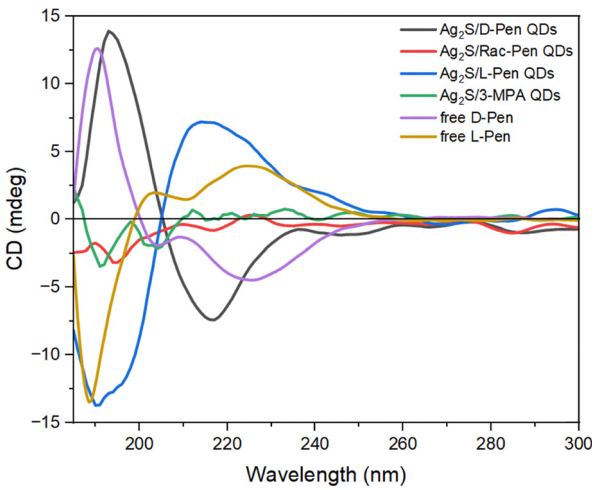

Fig. 3 CD spectra of Ag_2S/D-Pen, Ag_2S/*Rac*-Pen, Ag_2S/L-Pen and Ag_2S/3-MPA QDs and their corresponding ligands (free D-/L-Pen) measured in aqueous solution.

ligand (3-mercaptopropionic acid, 3-MPA), which is achiral (green curve, Fig. 3). As expected, no CD signal was observed. This confirms the hypothesis that the observed chirality stems mainly from the ligand and the changes in chirality result from its interactions with QD, with a contribution caused by the distortion of surface atoms upon the chiral ligand adsorption.[1] The detailed mechanism responsible for inducting chirooptical activity has been well described in the literature, see ref. 48, 68 and 69 Pioneering work by Moloney's group on CdS QDs,[69] based on density functional theory (DFT) calculations, demonstrated that the spatial arrangement of Cd atoms on the QD surface undergoes significant chiral distortion under the influence of Pen ligands, resulting in the formation of a chiral structure within the surface layer. Later studies confirmed this mechanism. For instance, Guangmin *et al.*[48] showed that the thiol group of Cys can induce chiral distortions of the CdTe surface and, additionally, affect the optical properties of the QDs by inducing orbital hybridization, resulting in shifts in their absorption and emission spectra.

Inspired by the studies of Moloney's group,[51] we conducted a CD experiment monitoring the formation of Ag_2S QDs stabilized by L-Pen at pH = 12 (Fig. 4). A detailed analysis at each stage of the synthesis enabled the identification of the origin of the band at ~215 nm. It was attributed to the free L-Pen absorption band, red-shifted by approximately 10 nm, indicating an interaction between L-Pen and the QD surface. Additionally, setting the pH to 12 caused a sudden shift of the entire spectrum by 7 nm toward longer wavelengths (Fig. 4(a)). This shift is likely due to the deprotonation of functional groups.[70–72] The next step involved the addition of $AgNO_3$, which resulted in a shift of the CD signal from 230 nm to 218 nm along with a decrease in the amplitude between the CD maximum and minimum. These changes were attributed to the initial formation of a complex between L-Pen and silver ions[51] (Fig. 4(b)). The subsequent addition of Na_2S, leading to the formation of QDs, caused a blue shift of the spectrum of approximately 4 nm for both the maximum and minimum and the appearance of bands at 245 nm and 266 nm (Fig. 4(c)). In the following step we monitored the reaction progress at 90 °C, with CD measurements taken every 30 minutes from aliquots withdrawn from the reaction flask. The CD spectra revealed that, over time, the maximum and minimum bands gradually shifted closer together (Fig. 4(d)). Conducting the reaction at an elevated temperature (90 °C) may induce further structural changes and influence the adsorption of the chiral ligand on the QDs surface. Over time, ligand reorganization on the nanoparticle surface may occur, leading to spectral shifts and changes in optical activity due to the increasing particle size.[73] The gradual closing of the maximum and minimum bands may indicate the progressive stabilization of the system.

No chiroptical activity was detected in the NIR emission region. Based on previous reports for Pen-stabilized QDs,[51] significant circularly polarized luminescence (CPL) activity is not expected due to limited chirality transfer from surface ligands to achiral semiconductor dot core.

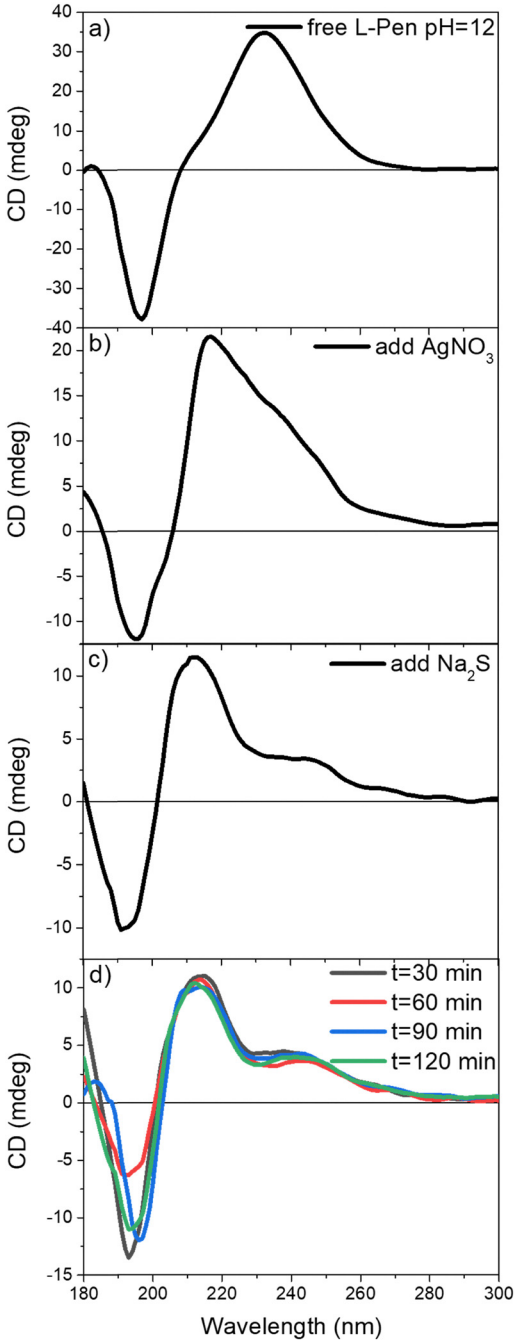

Fig. 4 CD monitoring of the formation of Ag_2S QDs stabilized with L-Pen. (a) Free Pen at pH = 12, (b) after addition of $AgNO_3$, (c) after subsequent addition of Na_2S, (d) spectra of samples withdrawn from the reaction flask measured after every 30 minutes.

Effect of synthetic parameters on the optical and photophysical properties of Pen-capped Ag_2S QDs

(a) Effect of reaction temperature. Reaction temperature has a significant impact on the size and, consequently, on the optical properties of Ag_2S QDs stabilized with D-, L-, and *Rac*-Pen. An increase in synthesis temperature from 50 to 90 °C led to a growth in nanoparticle size by approximately 0.3–0.5 nm in

the case of D-Pen and L-Pen stabilized QDs (samples D-2a/D-2b and L-2a/L-2b, respectively).

While D- and L-Pen showed a consistent temperature-dependent size increase, the behavior of QDs stabilized with *Rac*-Pen occasionally diverged from this trend. In certain cases, higher temperatures did not necessarily lead to larger QDs.

In order to elucidate an underlaying mechanism this behavior, the optical properties of the samples were compared. The normalized emission spectra (Fig. 5) revealed subtle differences in the peak shift of the emission (hypsochromic shift) which may be attributed to the complementary nature of D- and L-Pen molecules. This interaction could promote tighter packing of the stabilizer on the surface of Ag_2S/*Rac*-Pen QDs, potentially limiting nanocrystal growth, as previously suggested by Moloney.[51]

Absorption spectra (Fig. S2 and Section S2 in SI) displayed a pronounced red-shift in onset wavelength with increasing temperature (particularly evident for 4a* and 4b samples), consistent with crystallite growth. This phenomenon aligns with reports in the literature.[12,74] Fluorescence measurements further support this trend. Normalized emission spectra (Fig. 5(a–d) and S3, Section S3 in SI) showed a red-shift of the emission band with increasing temperature, which is attributed to quantum confinement effects, where the band gap energy narrows as QD size increases.[14]

(b) Effect of Ag : S molar ratio. Variation in the Ag : S molar ratio during synthesis had a pronounced effect on both the structural and spectroscopic properties of the Ag_2S QDs. Generally, raising the Ag : S ratio from 2 to 4 resulted in reduction in average QDs size. This trend is clearly observed for samples synthesized at 90 °C (2b *vs.* 4b), where TEM analysis shows consistently larger nanocrystals for Ag : S = 2 compared to Ag : S = 4 (Table 1).

For samples synthesized at 50 °C (2a *vs.* 4a*), the size dependence on the Ag : S ratio is not visible, because sample 4a* could not be purified by centrifugation. The presence of smaller, incompletely formed QDs and possible aggregates may affect the accuracy of the average size determination by TEM analysis.

Despite these limitations, the overall trend observed for the purified series indicates that a lower Ag : S ratio (Ag : S = 2) favors the formation of larger QDs, and this tendency is generally consistent across the three Pen variants.

The changes in QD size due to the Ag : S ratio are also reflected in the optical spectra. As shown in Fig. S2 (Section S2 in SI) and Fig. 5, samples prepared with an Ag : S ratio of 2 exhibited bathochromic shifts in both absorption and emission profiles, confirming the formation of larger QDs under these conditions (see Table 1 for wavelength details).

The shifts in spectral features observed for different Ag : S ratios correlate with trends in fluorescence lifetimes; as it is discussed later in Section (e).

(c) Effect of reaction time. Reaction time plays a critical role in determining the optical quality and structural characteristics of Ag_2S QDs, primarily by governing the extent of nanocrystal growth and the evolution of quantum confinement effect. As the reaction proceeds, the size of QDs typically increases, which in turn reduces the band gap energy and shifts absorption and emission spectra toward longer wavelengths. However, prolonged reaction time may also lead to undesirable effects, such as reduced luminescence efficiency or structural degradation. A key trend observed across all stereoisomers of Pen is that shorter reaction times generally favor the formation of smaller, better-confined QDs, which exhibit more pronounced excitonic features and longer fluorescence lifetimes. Table S1 (Section S4 in SI) summarizes the dependence of the key parameters on the reaction time. This relationship is particularly evident at lower temperatures (50 °C), where the formation and preservation of well-defined exciton bands are possible. Absorption spectra collected over time (Fig. S4 and Section S5 in SI) show that in all samples, exciton bands emerge within the first 30 minutes and evolve depending on the temperature and ligand type. For example, in D-Pen and *Rac*-Pen Ag_2S QDs samples at 50 °C, the exciton bands are well defined up to 90 min, suggesting progressive and controlled growth of small, monodisperse QDs. In contrast, for L-Pen Ag_2S QDs, the band weakens or vanishes with time, especially at 90 °C, indicating excessive growth or loss of quantum confinement.

Emission spectra (Fig. S5 and Section S5 in SI) further support this trend, a gradual red-shift of the emission maximum with increasing reaction time is observed, particularly at elevated temperatures. This red-shift reflects the increase in particle size and reduction in band gap, but also correlates with a decline in fluorescence intensity, likely due to structural defects and trap formation, as discussed earlier. Crucially, these findings indicate that reaction time must be carefully balanced: (a) if too short, the QDs may remain insufficiently developed, resulting in poorly defined excitonic features and reduced luminescence performance; (b) if too long, it promotes growth beyond the quantum confinement regime and increases

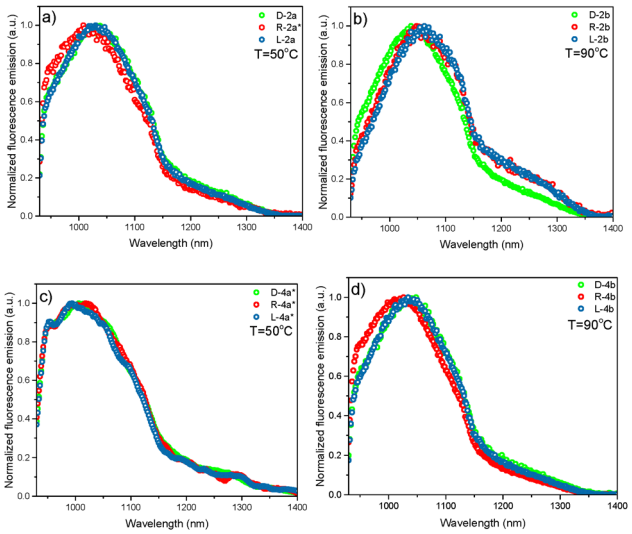

Fig. 5 Normalized emission spectra for Ag_2S/Pen QDs excited at λ = 500 nm.

the likelihood of trap states or agglomeration, both of which reduce luminescence performance. The exciton Bohr radius, which is the characteristic size of an exciton serving a fundamental length scale for describing quantum confinement effects, has been theoretically calculated and experimentally determined for Ag_2S QDs to be approximately 2.2 nm.[14] This relatively small exciton Bohr radius of Ag_2S semiconductor means that the quantum confinement effect becomes significant for nanocrystals close to this size, leading to changes in their optical properties.

(d) Effect of purification method. The purification process plays an essential role in determining the optical quality of Ag_2S QDs. In particular, ethanol-assisted centrifugation proved to be an effective method for removing unreacted precursors, side products, and the smallest, weakly passivated QDs, which would otherwise deteriorate the spectroscopic and emissive properties of the nanocrystals.

Absorption spectra reveal that the exciton band structure is most clearly visible in samples that could not be centrifuged (Fig. S2, samples 4a marked with "*"), suggesting that these samples contain small, well-defined QDs with relatively narrow size distribution. In contrast, the vanishing of the exciton band in centrifuged samples is indicative of broader size dispersion. According to Smirnov,[35] for samples with QD size dispersion above 25%, the ground state exciton absorption band does not have a pronounced peak, supporting the conclusion that increased polydispersity and sizes contribute to the loss of excitonic structure in UV-Vis spectra. This means that during the centrifugation purification process, not only by-products but also the smallest QDs remain in the supernatant. This conclusion is supported by TEM images and measurements of the QD diameters (3.6 ± 0.6 nm and 2.9 ± 0.5 nm for L-2a and its supernatant, respectively). However, a well-visible exciton peak, which indicates small and high-quality QDs, is not confirmed by the emission properties.

Emission spectra presented in Fig. 6 show a bathochromic shift of 5-10 nm for centrifuged samples compared to their unpurified counterparts. This shift reflects the removal of smaller QDs, resulting in a more uniform population of slightly larger QDs.

These findings also help explaining the challenges in centrifugation encountered for samples synthesized in low Ag : S ratios and temperatures (samples 4a, T = 50 °C, Ag : S = 4), where the formation of very small QDs is expected. Under these conditions, very small amounts of QDs or very small sizes of QDs are obtained. These conditions may also be insufficient for the growth and effective passivation of Ag_2S QDs.

Further support for the effectiveness of centrifugation comes from fluorescence lifetime data (Table S2 and Section S6 in SI). Purified samples consistently exhibited longer average lifetimes, suggesting lower densities of surface defects and reduced non-radiative recombination.

To further investigate the impact of residual supernatant, an additional experiment was conducted: the supernatant from the first centrifugation was recentrifuged, and the resulting pellet was redispersed and added back to the purified sample

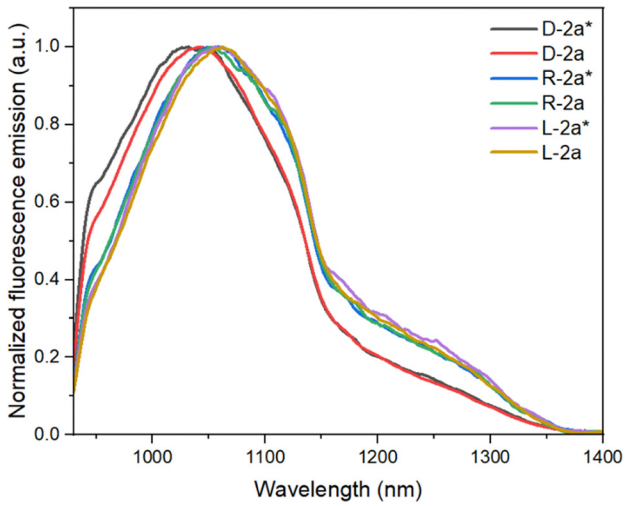

Fig. 6 Normalized fluorescence emission spectra of Ag_2S/Pen QDs, purified by centrifugation and not centrifuged (marked as 2a*), excited at λ = 500 nm.

(Section S7). This led to a measurable decrease in fluorescence lifetime, from 48.0 ns to 41.7 ns, despite only minimal dilution. This results confirms that unpurified solutions of Ag_2S/Pen QDs contain small, poorly passivated QDs and reaction by-products, both of which reduce luminescence performance.

(e) Influence of reaction conditions on photoluminescence lifetimes. A significant effect of reaction conditions on photoluminescence lifetimes was observed. Room temperature fluorescence decay curves of QDs synthesized under different conditions are shown in Fig. 7. Detailed data on lifetimes, amplitudes of individual components, fitting parameters and the *Rac* of Pen, obtained under specific conditions, are presented in Table 2.

To accurately determine lifetime values, fluorescence decay data were fitted using a three-exponential model, similar to

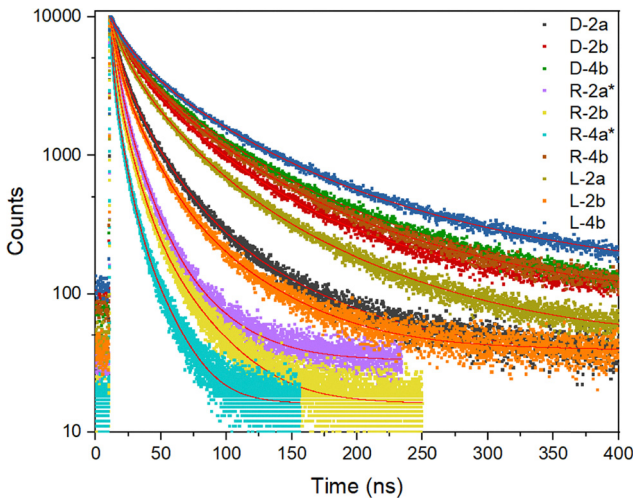

Fig. 7 The fluorescence decays of colloidal solutions of Ag_2S/Pen QDs with fitted curves (red lines).

Table 2 Fluorescence lifetime (τ) components, along with their respective amplitudes (A) and the correlation coefficient (χ^2) for Ag_2S/Pen QDs

Coating/sample number	τ_1 [ns]	τ_2 [ns]	τ_3 [ns]	A_1 [%]	A_2 [%]	A_3 [%]	$\tau_{average}$ [ns]	Correlation coefficient $(\chi^2)_{3\text{-exponential decay}}$
D-Pen								
D-2a	66.6	20.5	6.0	28.30	53.63	18.07	30.9	1.0990
D-2b	106.1	38.1	11.3	31.71	54.47	13.81	55.9	1.0670
D-4a*	23.4	7.7	2.2	29.70	51.17	19.13	11.3	1.1050
D-4b	135.0	47.0	13.2	32.91	52.88	14.21	71.1	1.0450
Rac-Pen								
R-2a*	32.8	11.7	4.1	20.75	53.65	25.59	14.1	1.0700
R-2b	31.0	9.6	2.8	25.09	55.13	19.77	13.6	1.1540
R-4a*	5.8	18.1	1.5	52.94	30.67	16.38	8.9	1.1800
R-4b	126.4	42.9	12.2	32.38	53.12	14.50	65.5	1.0360
L-Pen								
L-2a	30.7	89.5	9.1	51.64	34.52	13.84	48.0	1.0620
L-2b	53.4	16.9	4.9	29.45	53.56	16.99	25.6	1.0990
L-4a*	24.3	7.7	2.0	27.32	53.19	19.49	11.1	1.2210
L-4b	13.6	151.7	51.6	11.82	37.11	51.08	84.3	1.0570

other reports.[24,40,75] Biexponential fitting is commonly used in the analysis of Ag_2S QDs,[75,76] typically revealing two components (τ_1 and τ_2) corresponding to fast and slow decay pathways. The fastest decay emission components reflect the radiative relaxation of the electrons in their excited core-states to the ground state, *i.e.*, to core-state recombination. The longest lifetime components are due to radiative recombination involving shallow trap states.[24] It should be emphasied that the biexponential fitting of the decay curves in Ag_2S QDs does not necessarily reflect only two discrete relaxation pathways.[40] Instead, the observed nonexponential behavior is predominantly attributed to variations in nonradiative decay rates, influenced by differences in surface defect densities across QD formulations. Importantly, such nonexponential decay dynamics are evident even in Ag_2S nanocrystals with high emission efficiency.[75]

Such complex relaxation dynamics is not unique to Ag_2S QDs and has been widely reported in other QD systems, including CdSe,[77,78] ZnS/CdSe,[24] CdS[77] and GaSe.[77] As discussed earlier, surface defects introduce shallow and deep trap states within the band gap, which disturb emission dynamics. Upon excitation, electrons are promoted to higher energy levels within the conduction band (CB) of QDs, followed by rapid relaxation to the CB minimum. Radiative recombination with holes from this state leads to excitonic emission, typically corresponding to the fastest lifetime components. However, some electrons may become localized in shallow trap states within the CB, from which they may either thermally return to the CB or relax into deeper trap states. These pathways facilitate non-radiative recombination, ultimately reducing the QY.[78] Additionally, the presence of dark exciton states can also lead to further extension of lifetimes.[75,77] The combination of these overlapping processes, along with the inhomogeneity of nanocrystals in the sample, results in the emergence of multicomponent, most often multiexponential emission dynamics observed on the nanosecond scale.

Accordingly, the use of more complex fitting models, such as three- or even four-exponential functions, is not uncommon.[24,78,79] For instance, satisfactory fits to CdSe and ZnS/CdSe QDs decay curves were reported using models with four exponential components.[77]

In our analysis, fitting with three components was essential to capture meaningful differences between samples. Simpler models led to poor fit quality, reflected in significantly higher χ^2 values (see Table S4 and Section S8 in SI). Consequently, the curves were analyzed using the following equation:

$$I(t) = A_1 e^{-t/\tau_1} + A_2 e^{-t/\tau_2} + A_3 e^{-t/\tau_3} \quad (1)$$

where A_1, A_2 and A_3 are the amplitudes of the three components and τ_1, τ_2 and τ_3 are their corresponding lifetime values.

The longest fluorescence decay component was 151.7 ns (L-4b); two intermediate lifetime components were, on average, three times shorter and ten times shorter than the longest lifetime. The shortest decay component was approximately 1.51 ns (R-4a*). Average lifetimes varied notably: from 8.9 ns (R-4a*) to 84.3 ns (L-4b), the latter being the longest reported average lifetime for aqueous colloidal Ag_2S QDs. For comparison Table 3 compiles average lifetime values reported for Ag_2S QDs with various surface coatings.

Experimental results clearly indicate that elevated reaction temperature (T = 90 °C) combined with a Ag:S ratio of 4 significantly enhances lifetimes, regardless of the coating conformation (4b samples). This highlights the critical role of temperature in tuning the luminescence properties of QDs. Additionally, it was expected that the D- and L-stereoisomers of Pen would exhibit similar fluorescence lifetimes, however, despite identical synthesis conditions, different average decay times were recorded suggesting that the chirality of the surface ligand can affect the surface passivation efficiency and recombination processes in nanostructures.

(f) Quantum yield measurements. To complement the characterization of the emissive properties of Ag_2S/Pen QDs, QY measurements were conducted for samples synthesized under optimized conditions – both, at Ag:S molar ratios of

Table 3 Lifetime values reported for Ag_2S QDs with different coatings in aqueous and organic phases

Synthesis method	Ag^+ source	S^{2-} source	Phase/dispersant	Coating	QY [%]	$\lambda_{em,max}$ [nm]	$\tau_{average}$ [ns]	Ref.
Hydrothermal	$AgNO_3$	$Na_2S{\cdot}9H_2O$	Water	Pen	1.1	1037	84	This work
Hydrothermal	$AgNO_3$	$Na_2S{\cdot}9H_2O$	Water	2-MPA	—	984	41	35
Hydrothermal	$AgNO_3$	$Na_2S{\cdot}9H_2O$	Water	L-NIBC	0.04	1060	33	36
Microwave-assisted hydrothermal approach	$AgNO_3$	$Na_2S{\cdot}9H_2O$	Water	L-GSH	0.03–0.62	930–1200	143–265	40
Hydrothermal	$AgNO_3$	$Na_2S{\cdot}9H_2O$	Water	D-NIBC	0.11	1060	19	36
Heat-up (thermal decomposition)	$AgNO_3$	$Na_2S{\cdot}9H_2O$	Water	HSA	1.26–1.32	1060	—	80
Heat-up (thermal decomposition) and sonochemical surface etching	AgDDTC	DT	Organic ($CHCl_3$)	OLA	10	1200	1702	34
Heat-up (thermal decomposition)	AgDDTC	DT	Organic ($CHCl_3$)	DT	2.30	1220	1200	16
Heat-up (thermal decomposition)	AgDDTC	DT	Organic ($CHCl_3$)	DT	—	975–1175	57–181	14
Heat-up (thermal decomposition)	AgDDTC	DT	Organic ($CHCl_3$)	DT/C18PMH/PEG	17 in water)	1100	61	81
Seeded growth	AgAc, AgOA	$(TMS)_2S$	Organic (*n*-hexane)	MUA	0.15 (in water)	813	57	12
Hot injectrion	$AgNO_3$	TAA	Organic ($CHCl_3$)	OLA	—	1200	—	82
Heat-up (thermal decomposition)	AgDDTC	DT	Organic (water + $CHCl_3$)	HS-PEG	—	1200	28	39
Heat-up (thermal decomposition)	AgDDTC	DT	Water	HS-C_{11}-PEG	4.80 (in water)	1200	81	39
Heat-up (thermal decomposition)	AgDDTC	DT	Organic ($CHCl_3$)	DT	2.30	1220	1200	16

Abbreviations: DT: 1-dodecanethiol, $CHCl_3$: chloroform, Pen: penicillamine, 2-MPA: 2-mercaptopropionic acid, L-GSH: L-glutathione, D-/L-NIBC: *N*-isobutyryl-D/L-cysteine, HSA: human serum albumin, OLA: oleylamine, C_{18}PMH/PEG: poly(maleic anhydride-*alt*-1-octadecene)-polyethylene glycol, AgAc: silver(I) acetate, AgOA: silver(I) oleate, MUA: 11-mercaptoundecanoic acid, TAA: thioacetamide, HS-PEG: methoxy polyethylene glycol thiol.

Table 4 Fluorescence properties of chiral Ag_2S/Pen QDs under optimal synthesis conditions

Coating/sample number	Ag : S	*T* [°C]	Rxn time [min]	$pH_{(after)}$	Zeta pot. (mV)	Size (nm)	QY [%]	$\tau_{average}$ 3-exponential decay [ns]	Correlation coefficient $\chi^2_{3\text{-exponential decay}}$
D-Pen *t* = 60 min	2	50	60	11.9	−52.69	—	0.5	73.0	1.0330
D-4b	4	90	120	11.6	−36.16	3.7	1.1	71.1	1.0450
Rac-Pen *t* = 30 min	2	50	30	11.8	−28.97	—	0.8	68.2	1.0550
R-4b	4	90	120	11.4	−34.33	3.6	0.8	65.5	1.0360
L-2a	2	50	120	11.7	−41.18	3.6	0.5	48.0	1.0620
L-4b	4	90	120	11.4	−31.92	3.3	0.6	84.3	1.0570

4 (samples 4b) and 2 (D-Pen *t* = 60 min, *Rac*-Pen *t* = 30 min, and L-2a). The normalized emission spectra are presented in Fig. S7 (Section S9 in SI) together with their corresponding absorption spectra. All selected samples exhibited high colloidal stability and prolonged fluorescence lifetimes. The QY values, summarized in Table 4, range from 0.5% to 1.1% for aqueous colloidal Ag_2S QDs emitting in the NIR-II window. These are relatively high values, considering the emission spectral range and the fact that QDs with comparable or even ten times lower efficiency have been successfully used in *in vivo* imaging.[36,83,84] Previous studies, such as that by Moloney *et al.*,[51] have shown that the use of Pen as a ligand can significantly enhance QY; for instance, CdS/Pen QDs achieved a QY of 20 ± 4%. In the study by Shang *et al.*,[36] higher QY values were observed for the D-Pen conformer; however, we are cautious in definitively stating which enantiomer exhibits higher QY, as it depends on the QDs preparation conditions.

The noticeable lack of linearity between QY and fluorescence lifetimes may be due to the fact that the decay curves do not include all non-radiative processes.[75] As explained in the work of de Wit *et al.*, the so-called very fast direct quenching may lead to a decrease in QY, but this effect could occur too rapidly to be captured by lifetime measurement excited by the ps source and may be obscured in decay curves when measured with insufficient time resolution.

NLO properties of Ag_2S/Pen QDs

Among the optimized Ag_2S/Pen QDs, we selected those showing the highest stability and the most interesting optical properties for further characterization of NLO properties and cytotoxicity (*i.e.*, samples D-4b and L-4b).

To investigate the spectrally resolved NLO properties of Ag_2S QDs, the tunable femtosecond laser Z-scan technique was employed, enabling the determination of parameters like the two-photon absorption cross-section (σ_2).

Unlike many previous studies limited to a single excitation wavelength, our measurements were performed over a broad spectral range (VIS-NIR), providing a full 2PA spectrum for Ag_2S QDs functionalized with D-Pen and L-Pen, (Fig. 8) similar to earlier results for MPA-stabilized QDs.[57,63] This approach also allows us to compare the role of the ligand in shaping the NLO properties of Ag_2S QDs. As observed previously for Ag_2S QDs stabilized with MPA, 1PA SAT and 2PA effects are present. For shorter excitation wavelengths (600–725 nm for Ag_2S/L-Pen and up to775 nm for Ag_2S/D-Pen), only 1PA SAT was observed. Similar to the MPA-stabilized QDs, 2PA-related features began

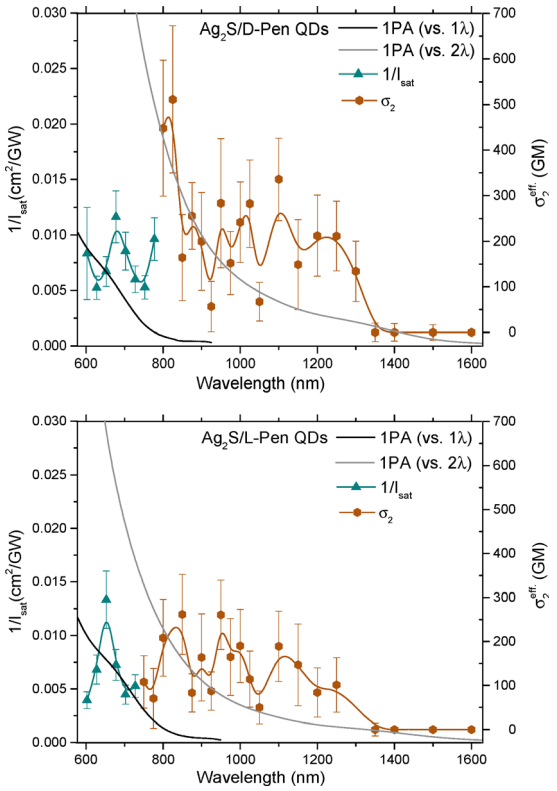

Fig. 8 Spectral dependence of σ_2^{eff} and $1/I_{sat}$ (reciprocal of 1PA saturation intensity) for Ag_2S/D-Pen and Ag_2S/L-Pen QDs. The σ_2^{eff} values are plotted as orange filled circles (the orange solid line is used to guide the eye, bars represent standard deviation). The values of $1/I_{sat}$ are plotted as green filled triangles (the green line is used to guide the eye). The black line represents the 1PA spectrum plotted *vs.* λ, and the grey line represents the same 1PA spectrum plotted *vs.* 2λ.

to emerge at wavelengths around 750 nm. However, unlike the earlier MPA-based system, where the 2PA activity was limited to a relatively narrow range (up to ~950 nm), the Pen-stabilized QDs exhibited a significantly broader 2PA response. Specifically, a pronounced 2PA contribution was observed in the range of 800–1300 nm for D-Pen and 750–1250 nm for L-Pen, respectively. The highest value of σ_2 was recorded for the Ag_2S/D-Pen QDs sample, reaching 511 GM at $\lambda_{EXC.}$ = 824 nm. For Ag_2S/L-Pen QDs, a maximum σ_2 value of 251 GM was observed at $\lambda_{EXC.}$ = 850 nm, along with an additional peak of 260 GM at $\lambda_{EXC.}$ = 950 nm. These results indicate that the D-Pen-stabilized QDs exhibit nearly double the 2PA efficiency of their L-Pen counterparts, despite having comparable physicochemical properties.

To evaluate and compare the nonlinear absorption performance of the studied systems, the factor of merit σ_2/M was calculated. For Ag_2S/D-Pen QDs at $\lambda_{EXC.}$ = 824 nm, the value reached 0.005 GM mol g^{-1}, while for Ag_2S/L-Pen QDs at $\lambda_{EXC.}$ = 850 and 950 nm it was 0.003 GM mol g^{-1}. Although these values are lower than those reported for Ag_2S/MPA QDs[57] (0.013 GM mol g^{-1}), and CdS QDs[85] (0.038 GM mol g^{-1}), the Ag_2S/Pen QDs system remains highly promising due to its tunability and potential for enhancement.[86–88] Our recent studies[63] have shown that strategic modifications, such as attaching Ag_2S QDs to nanoshell surfaces or embedding them in silica nanospheres decorated with gold nanoislands can significantly amplify the 2PA response. These approaches offer a viable path toward increasing the σ_2/M factor and unlocking the full potential of Ag_2S/Pen QDs for advanced photonic and bioimaging applications.

Cytotoxic properties of the Ag_2S/Pen QDs

The biocompatibility and cytotoxic potential of biosynthesized Ag_2S/Pen QDs were systematically evaluated using two physiologically relevant cell models representing distinct cellular environments: THP-1 macrophages and HLMEC endothelial cells. The MTT assay was employed to assess cellular metabolic activity as an indicator of cell viability following Ag_2S/D-Pen and Ag_2S/L-Pen QDs exposure.

Cytotoxicity in THP-1 macrophages

THP-1 cells, differentiated into macrophages using PMA treatment, demonstrated remarkable tolerance to Ag_2S/Pen QD exposure across all tested concentrations (Fig. 9(a)). Both Ag_2S/D-Pen and Ag_2S/L-Pen QDs showed no cytotoxic effects, with cell viability consistently maintained between 95–105% relative to untreated controls across the entire concentration range (0.001–1 mg mL^{-1}). This indicates high biocompatibility of the synthesized QDs with macrophage cells. Interestingly, the free amino acids D- and L-Pen exhibited significant proliferative effects on THP-1 macrophages. At the highest concentrations (1 mg mL^{-1}), both Pen isomers enhanced cellular metabolic activity, with cell viability reaching 120–140% of control values ($p < 0.005$). This proliferative response may be attributed to the antioxidant properties of Pen, which could stimulate macrophage activation and metabolic enhancement. The robust tolerance of macrophages to QDs exposure aligns with their physiological role as professional phagocytes equipped with enhanced antioxidant defence mechanisms and efficient particle clearance capabilities. This finding suggests potential compatibility of these QDs with immune system components, which is crucial for biomedical applications.

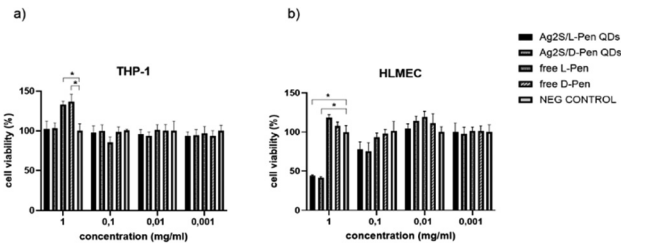

Fig. 9 Cytotoxicity assessment of Ag_2S/D-Pen QDs and Ag_2S/L-Pen QDs and free D-/L-Pen in human cell models. Cell viability was determined using MTT assay after 48-hour exposure to various QD concentrations. (a) THP-1 macrophages showed no cytotoxic effect across all tested concentrations for QDs formulations, while L-Pen and D-Pen demonstrated proliferative effects (*$p < 0.005$); (b) HLMEC endothelial cells demonstrated concentration-dependent sensitivity with significant cytotoxicity at 1 mg mL^{-1} (*$p < 0.001$). Data represent mean ± SD.

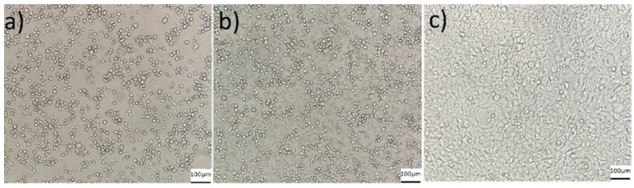

Fig. 10 Morphological assessment of HLMEC cells following Ag_2S/Pen QDs exposure. Representative inverted light microscopy images of cell morphology after 48-hour incubation with QDs. Images show cells treated with (a) Ag_2S/D-Pen QDs, (b) Ag_2S/L-Pen QDs, and (c) control (non-treated cells/water). Morphological alterations were observed in QDs treated groups (panel a and b), with cells appearing rounded and less adherent to the surface compared to control cells which maintained typical spread morphology and confluent monolayer formation.

Cytotoxicity in HLMEC endothelial cells

HLMEC endothelial cells exhibited a markedly different response pattern compared to macrophages, demonstrating concentration-dependent sensitivity to QDs (Fig. 9(b)). At the highest concentration tested (1 mg mL^{-1}), significant cytotoxic effect was observed for Ag_2S/Pen QDs treatments, with cell viability decreasing to approximately 40–50% of control values ($p < 0.001$). However, at concentrations ≤ 0.1 mg mL^{-1}, HLMEC cells maintained acceptable viability levels ($>80\%$), suggesting a clear dose-dependent toxicity threshold. The enhanced sensitivity of endothelial cells compared to macrophages reflects fundamental differences in cellular physiology and defence mechanisms. Endothelial cells, which form the vascular barrier and regulate blood-tissue exchange, may be more susceptible to nanoparticle-induced stress due to their specialized barrier functions and metabolic requirements (Fig. 10).

Summary and conclusions

In this study, we present the hydrothermal synthesis and comprehensive characterization of water-soluble Ag_2S QDs stabilized with Pen ligands. By systematically varying reaction temperature, time, and the Ag : S molar ratio, we evaluated how synthesis parameters influence QDs size, structure, and resulting optical properties. The optimized conditions (summarized in Table 4) enabled the production of QDs with strong emission in the NIR-II range ($\sim$1040 nm), high colloidal stability, and relatively high QY, considering the emission wavelength. Fluorescence lifetime measurements revealed decay times reaching 84 ns in aqueous solution, which is one of the best results in this range.

A comparative analysis of QDs stabilized with D-, L-, and racemic Pen allowed assessment of how ligand stereochemistry affects QDs morphology and both linear and NLO responses.

The NLO properties of Ag_2S/Pen QDs were evaluated using the Z-scan technique. The peak σ_2 values were determined to be 511 GM (at $\lambda_{EXC.}$ = 824 nm) for Ag_2S/D-Pen 260 GM (at $\lambda_{EXC.}$ = 950 nm) for Ag_2S/L-Pen, suggesting their potential applicability in NLO, for example in TPFM.

Finally, cytotoxicity assays confirmed the low toxicity of Ag_2S/Pen QDs. Interestingly, no significant differences in cytotoxicity were observed between the enantiomers, in contrast to other chiral QDs described in the literature.

These results indicate that appropriate selection of the surface ligand structure, including its chiral configuration, can be an effective tool for modulating the structural and photophysical properties of QDs. This study contributes to the design of stable NIR-emitting nanomaterials for potential biomedical and photonic applications.

Conflicts of interest

There are no conflicts to declare.

Data availability

All relevant experimental supporting this study are provided in the supplementary information (SI), which includes XRD patterns of the prepared Ag_2S quantum dots (S1); absorbance spectra of Ag_2S/Pen QDs under varied synthesis conditions (S2); emission spectra of Ag_2S/Pen QDs under varied synthesis conditions (S3); the effect of reaction time on the optical properties of Ag_2S/Pen QDs (S4); time-dependent absorbance and emission spectra (S5); fluorescence decay times of centrifuged *versus* non-centrifuged samples (S6); a comparison of centrifuged QDs and re-centrifuged supernatant (S7); bi-exponential fitting of fluorescence decay times (S8); absorbance and normalized emission spectra for optimized synthesis conditions (S9); detailed fluorescence decay information for reactions conducted at different times and temperatures (S10); and fit residuals for the fluorescence lifetime data (S11). See DOI: https://doi.org/10.1039/d5tc04053a.

The raw data are available in the institutional repository at https://uwr.rodbuk.pl/.

Acknowledgements

This work was supported by the project no. UMO-2021/43/D/ST5/02249, SONATA 17, funded by National Science Center Poland (NCN). M. G.-W. acknowledges the support of the University of Wrocław under the program ''Initiative of Excellence Research University'' for funding the academic visit to a leading international institution (Agreement No. IDUB.29/2024). J. T. acknowledges the support of the student grant awarded under the ''Excellence Initiative-Research University'' program at the University of Wrocław (Grant No. 0320/2020/20). M. N. and M. S. acknowledge support from the National Science Centre Poland under grant no. UMO-2023/49/B/ST11/01536.

References

1 G. Li, J. Zheng, J. Li, J. Kang, X. Jin, A. Guo, Z. Chen, X. Fei, K. Wang, H. Liu, H. Zhao, W. Liu and G. Yang, *J. Mater. Chem. C*, 2024, **12**, 10825–10836.

2 M. Sobiech, P. Luliński, P. P. Wieczorek and M. Marć, *TrAC, Trends Anal. Chem.*, 2021, **142**, 116306.
3 M. S. Freire, H. J. B. Silva, G. M. Albuquerque, J. P. Monte, M. T. A. Lima, J. J. Silva, G. A. L. Pereira and G. Pereira, *Sci. Total Environ.*, 2024, **931**, 172848.
4 C. Ding, Y. Huang, Z. Shen and X. Chen, *Adv. Mater.*, 2021, **33**, 2007768.
5 R. Ding, Y. Chen, Q. Wang, Z. Wu, X. Zhang, B. Li and L. Lin, *J. Pharm. Anal.*, 2022, **12**, 355–364.
6 K. Zhang, F.-R. Chen, L. Wang and J. Hu, *Small*, 2023, **19**, 2206044.
7 O. E. Semonin, J. C. Johnson, J. M. Luther, A. G. Midgett, A. J. Nozik and M. C. Beard, *J. Phys. Chem. Lett.*, 2010, **1**, 2445–2450.
8 M. Greben, A. Fucikova and J. Valenta, *J. Appl. Phys.*, 2015, **117**, 144306.
9 B. Purushothaman and J. M. Song, *Biomater. Sci.*, 2021, **9**, 51–69.
10 M. S. Smirnov and O. V. Ovchinnikov, *J. Lumin.*, 2020, **227**, 117526–117533.
11 P. T. Buz, F. D. Duman, M. Erkisa, G. Demirci, F. Ari, E. Ulukaya and H. Y. Acar, *Nanomedicine*, 2019, **14**, 969–987.
12 P. Jiang, Z.-Q. Tian, C.-N. Zhu, Z.-L. Zhang and D.-W. Pang, *Chem. Mater.*, 2012, **24**, 3–5.
13 H. D. A. Santos, D. Ruiz, G. Lifante, C. Jacinto, B. H. Juarez and D. Jaque, *Nanoscale*, 2017, **9**, 2505–2513.
14 Y. Zhang, Y. Liu, C. Li, X. Chen and Q. Wang, *J. Phys. Chem. C*, 2014, **118**, 4918–4923.
15 H. D. A. Santos, I. Zabala Gutiérrez, Y. Shen, J. Lifante, E. Ximendes, M. Laurenti, D. Méndez-González, S. Melle, O. G. Calderón, E. López Cabarcos, N. Fernández, I. Chaves-Coira, D. Lucena-Agell, L. Monge, M. D. Mackenzie, J. Marqués-Hueso, C. M. S. Jones, C. Jacinto, B. del Rosal, A. K. Kar, J. Rubio-Retama and D. Jaque, *Nat. Commun.*, 2020, **11**, 2933.
16 A. Ortega-Rodríguez, Y. Shen, I. Zabala Gutierrez, H. D. A. Santos, V. Torres Vera, E. Ximendes, G. Villaverde, J. Lifante, C. Gerke, N. Fernández, O. G. Calderón, S. Melle, J. Marques-Hueso, D. Mendez-Gonzalez, M. Laurenti, C. M. S. Jones, J. M. López-Romero, R. Contreras-Cáceres, D. Jaque and J. Rubio-Retama, *ACS Appl. Mater. Interfaces*, 2020, **12**, 12500–12509.
17 D. Gerion, F. Pinaud, S. C. Williams, W. J. Parak, D. Zanchet, S. Weiss and A. P. Alivisatos, *J. Phys. Chem. B*, 2001, **105**, 8861–8871.
18 T. Jamieson, R. Bakhshi, D. Petrova, R. Pocock, M. Imani and A. M. Seifalian, *Biomaterials*, 2007, **28**, 4717–4732.
19 F. Pinaud, X. Michalet, L. A. Bentolila, J. M. Tsay, S. Doose, J. J. Li, G. Iyer and S. Weiss, *Biomaterials*, 2006, **27**, 1679–1687.
20 J. Chang, H. Xia, S. Wu and S. Zhang, *J. Mater. Chem. C*, 2014, **2**, 2939–2943.
21 S. He, L. Wang, X. Zhang, Y. Lv, Z. Zhou, R. Zhang, Y. Liang, G. Liang, J. Du and K. Wu, *Angew. Chem., Int. Ed.*, 2025, **64**, e202423960.
22 M. Dahan, T. Laurence, F. Pinaud, D. S. Chemla, A. P. Alivisatos, M. Sauer and S. Weiss, *Opt. Lett.*, 2001, **26**, 825–827.
23 H. Chang, J. Kim, S. H. Lee, W. Y. Rho, J. H. Lee, D. H. Jeong and B.-H. Jun, in *Nanotechnology for Bioapplications*, ed. B.-H. Jun, Springer, Singapore, 2021, vol. 1309, pp. 97–132.
24 M. J. Ruedas-Rama, A. Orte, E. A. H. Hall, J. M. Alvarez-Pez and E. M. Talavera, *Chem. Phys. Chem.*, 2011, **12**, 919–929.
25 D. R. Larson, W. R. Zipfel, R. M. Williams, S. W. Clark, M. P. Bruchez, F. W. Wise and W. W. Webb, *Science*, 2003, **300**, 1434–1436.
26 Y. Shen, A. J. Shuhendler, D. Ye, J.-J. Xu and H.-Y. Chen, *Chem. Soc. Rev.*, 2016, **45**, 6725–6741.
27 M. Karimi, P. Sahandi Zangabad, S. Baghaee-Ravari, M. Ghazadeh, H. Mirshekari and M. R. Hamblin, *J. Am. Chem. Soc.*, 2017, **139**, 4584–4610.
28 J. K. Zaręba, M. Nyk and M. Samoć, *Adv. Opt. Mater.*, 2021, **9**, 2100216.
29 L. Yun, Y. Qiu, C. Yang, J. Xing, K. Yu, X. Xu and W. Wei, *Photon. Res.*, 2018, **6**, 1028–1032.
30 R. Signorini, I. Fortunati, F. Todescato, S. Gardin, R. Bozio, J. J. Jasieniak, A. Martucci, G. Della Giustina, G. Brusatin and M. Guglielmi, *Nanoscale*, 2011, **3**, 4109–4113.
31 D. O. Oluwole, A. V. Yagodin, J. Britton, A. G. Martynov, Y. G. Gorbunova, A. Y. Tsivadze and T. Nyokong, *Dalton Trans.*, 2017, **46**, 16190–16198.
32 C. Livache, B. Martinez, N. Goubet, C. Gréboval, J. Qu, A. Chu, S. Royer, S. Ithurria, M. G. Silly, B. Dubertret and E. Lhuillier, *Nat. Commun.*, 2019, **10**, 2125.
33 H. He, Y. Lin, Z.-Q. Tian, D.-L. Zhu, Z.-L. Zhang and D.-W. Pang, *Small*, 2018, **14**, 1703296.
34 I. Z. Gutierrez, C. Gerke, Y. Shen, E. Ximendes, M. M. Silvan, R. Marin, D. Jaque, O. G. Calderón, S. Melle and J. Rubio-Retama, *ACS Appl. Mater. Interfaces*, 2022, **14**, 4871–4881.
35 M. S. Smirnov and O. V. Ovchinnikov, *J. Lumin.*, 2020, **227**, 117526.
36 S. Qu, Q. Jia, Z. Li, Z. Wang and L. Shang, *Sci. Bull.*, 2022, **67**, 1274–1283.
37 P. Jiang, C.-N. Zhu, Z.-L. Zhang, Z.-Q. Tian and D.-W. Pang, *Biomaterials*, 2012, **33**, 5130–5135.
38 G. Hong, S. Diao, J. Chang, A. L. Antaris, C. Chen, B. Zhang, S. Zhao, D. N. Atochin, P. L. Huang, K. I. Andreasson, C. J. Kuo and H. Dai, *Nat. Photonics*, 2014, **8**, 723–730.
39 M. Wang, S. Ling, Z. Zhang, Y. Zhang, H. Yang and Q. Wang, *Inorg. Chem. Front.*, 2025, **12**, 2954–2961.
40 O. El-Dahshan, A. Deniaud, W. L. Ling, K. D. Wegner, O. Proux, G. Veronesi and P. Reiss, *Nanoscale*, 2025, **17**, 14637–14646.
41 F. Zhu, X. Li, Y. Li, M. Yan and S. Liu, *Anal. Chem.*, 2015, **87**, 357–361.
42 M. Jakob, A. von Weber, A. Kartouzian and U. Heiz, *Phys. Chem. Chem. Phys.*, 2018, **20**, 20347–20351.
43 F. Li, Y. Li, X. Yang, X. Han, Y. Jiao, T. Wei, D. Yang, H. Xu and G. Nie, *Angew. Chem., Int. Ed.*, 2018, **57**, 2377–2382.
44 Y. Duan, L. Han, J. Zhang, S. Asahina, Z. Huang, L. Shi, B. Wang, Y. Cao, Y. Yao, L. Ma, C. Wang, R. K. Dukor, L. Sun, C. Jiang, Z. Tang, L. A. Nafie and S. Che, *Angew. Chem., Int. Ed.*, 2015, **54**, 15170–15175.

45 A. K. Visheratina, F. Purcell-Milton, R. Serrano-García, V. A. Kuznetsova, A. O. Orlova, A. V. Fedorov, A. V. Baranov and Y. K. Gun'ko, *J. Mater. Chem. C*, 2017, **5**, 1692–1698.
46 W. Ma, L. Xu, A. F. de Moura, X. Wu, H. Kuang, C. Xu and N. A. Kotov, *Chem. Rev.*, 2017, **117**, 8041–8093.
47 A. Ben Moshe, D. Szwarcman and G. Markovich, *ACS Nano*, 2011, **5**, 9034–9043.
48 G. Li, X. Fei, H. Liu, J. Gao, J. Nie, Y. Wang, Z. Tian, C. He, J.-L. Wang, C. Ji, D. Oron and G. Yang, *ACS Nano*, 2020, **14**, 4196–4205.
49 K. Ngamdee and W. Ngeontae, *Sens. Actuators, B*, 2018, **274**, 402–411.
50 C. Hao, R. Gao, Y. Li, L. Xu, M. Sun, C. Xu and H. Kuang, *Angew. Chem., Int. Ed.*, 2019, **58**, 7371–7374.
51 M. P. Moloney, Y. K. Gun'ko and J. M. Kelly, *Chem. Commun.*, 2007, 3900–3902.
52 L. Xiao, T. An, L. Wang, X. Xu and H. Sun, *Nano Today*, 2020, **30**, 100824.
53 Q. Ren, Y. Ma, S. Zhang, L. Ga and J. Ai, *ACS Omega*, 2021, **6**, 6361–6367.
54 I. Demirhan, M. Kanyalkar, A. Chandra, H. W. Doerr, E. Coutinho, J. Loewer, A. Saran and P. Chandra, *FEBS Lett.*, 2002, **516**, 43–46.
55 N. Suzuki, Y. Wang, P. Elvati, Z.-B. Qu, K. Kim, S. Jiang, E. Baumeister, J. Lee, B. Yeom, J. H. Bahng, J. Lee, A. Violi and N. A. Kotov, *ACS Nano*, 2016, **10**, 1744–1755.
56 Y. Li, Y. Zhou, H.-Y. Wang, S. Perrett, Y. Zhao, Z. Tang and G. Nie, *Angew. Chem., Int. Ed.*, 2011, **50**, 5860–5864.
57 M. Gordel-Wójcik, M. Malik, A. Siomra, M. Samoć and M. Nyk, *J. Phys. Chem. Lett.*, 2023, **14**, 11117–11124.
58 M. Gordel-Wójcik, J. Tracz, M. Malik, I. Czeluśniak and E. Zych, *Opt. Mater.*, 2024, **155**, 115831.
59 C. C. Chiu and L. T. Grady, in *Analytical Profiles of Drug Substances*, ed. K. Florey, R. Bishara, G. A. Brewer, J. E. Fairbrother, L. T. Grady, H.-G. Leemann, J. A. Mollica and B. C. Rudy, Academic Press, 1981, vol. 10, pp. 601–637.
60 B. O. Leung, F. Jalilehvand, V. Mah, M. Parvez and Q. Wu, *Inorg. Chem.*, 2013, **52**, 4593–4602.
61 M. Buljac, D. Krivić, I. Š. Rončević, N. Vladislavić and M. Buzuk, *Chemosensors*, 2022, **10**, 240.
62 M. P. Moloney, J. Govan, A. Loudon, M. Mukhina and Y. K. Gun'ko, *Nat. Protoc.*, 2015, **10**, 558–573.
63 M. Gordel-Wójcik, R. Kołkowski, M. Nyk and M. Samoć, *ACS Appl. Mater. Interfaces*, 2025, **17**, 28484–28494.
64 V. Nandwana, K. E. Elkins, N. Poudyal, G. S. Chaubey, K. Yano and J. P. Liu, *J. Phys. Chem. C*, 2007, **111**, 4185–4189.
65 H.-Y. Yang, Y.-W. Zhao, Z.-Y. Zhang, H.-M. Xiong and S.-N. Yu, *Nanotechnology*, 2013, **24**, 55706.
66 J. Mendes, K. J. de Almeida, J. L. Neto, T. C. Ramalho and H. A. Duarte, *Spectrochim. Acta, Part A*, 2017, **184**, 308–317.
67 H. Yao, N. Nishida and K. Kimura, *Chem. Phys.*, 2010, **368**, 28–37.
68 V. A. Kuznetsova, E. Mates-Torres, N. Prochukhan, M. Marcastel, F. Purcell-Milton, J. O'Brien, A. K. Visheratina, M. Martinez-Carmona, Y. Gromova, M. Garcia-Melchor and Y. K. Gun'ko, *ACS Nano*, 2019, **13**, 13560–13572.
69 S. D. Elliott, M. P. Moloney and Y. K. Gun'ko, *Nano Lett.*, 2008, **8**, 2452–2457.
70 G. Jung, M. Ottnad and M. Rimpler, *Eur. J. Biochem.*, 1973, **35**, 436–444.
71 R. Ding, J. Ying and Y. Zhao, *R. Soc. Open Sci.*, 2021, **8**, 201963.
72 C. Toniolo, *J. Phys. Chem.*, 1970, **74**, 1390–1392.
73 M. Farrag, *Mater. Chem. Phys.*, 2016, **180**, 349–356.
74 Y. He, Y. Zhong, Y. Su, Y. Lu, Z. Jiang, F. Peng, T. Xu, S. Su, Q. Huang, C. Fan and S.-T. Lee, *Angew. Chem., Int. Ed.*, 2011, **50**, 5695–5698.
75 J. W. de Wit, I. Zabala-Gutierrez, R. Marin, A. Zhakeyev, S. Melle, O. G. Calderon, J. Marques-Hueso, D. Jaque, J. Rubio-Retama and A. Meijerink, *J. Phys. Chem. Lett.*, 2024, **15**, 8420–8426.
76 E. N. Bodunov and A. L. Simões Gamboa, *J. Phys. Chem. C*, 2018, **122**, 10637–10642.
77 J. A. Kloepfer, S. E. Bradforth and J. L. Nadeau, *J. Phys. Chem. B*, 2005, **109**, 9996–10003.
78 I. S. Liu, H. H. Lo, C. T. Chien, Y. Y. Lin, C. W. Chen, Y. F. Chen and S. C. Liou, *J. Mater. Chem.*, 2008, **18**, 675–682.
79 F. D. Duman, R. Khodadust, E. G. Durmusoglu, M. B. Yagci and H. Y. Acar, *RSC Adv.*, 2016, **6**, 77644–77654.
80 T. Yang, Y. Tang, L. Liu, X. Lv, Q. Wang, H. Ke, Y. Deng, H. Yang, X. Yang, G. Liu, Y. Zhao and H. Chen, *ACS Nano*, 2017, **11**, 1848–1857.
81 F. Hu, C. Li, Y. Zhang, M. Wang, D. Wu and Q. Wang, *Nano Res.*, 2015, **8**, 1637–1647.
82 Y. Wang, X. Li, M. Xu, K. Wang, H. Zhu, W. Zhao, J. Yan and Z. Zhang, *Nanoscale*, 2018, **10**, 2577–2587.
83 L. Tan, A. Wan and H. Li, *ACS Appl. Mater. Interfaces*, 2014, **6**, 18–23.
84 P. Jiang, C.-N. Zhu, Z.-L. Zhang, Z.-Q. Tian and D.-W. Pang, *Biomaterials*, 2012, **33**, 5130–5135.
85 J. Szeremeta, M. Nyk, D. Wawrzynczyk and M. Samoć, *Nanoscale*, 2013, **5**, 2388–2393.
86 K. C. Nawrot, D. Wawrzyńczyk, O. Bezkrovnyi, L. Kępiński, B. Cichy, M. Samoć and M. Nyk, *Nanomaterials*, 2020, **10**, 715.
87 R. Kosman, D. Wawrzyńczyk, M. Nyk, M. Pawlyta, O. Bezkrovnyi and B. Cichy, *J. Mater. Chem. C*, 2023, **11**, 10758–10769.
88 M. Nyk, J. Szeremeta, D. Wawrzynczyk and M. Samoć, *J. Phys. Chem. C*, 2014, **118**, 17914–17921.